Size-based characterization of dendrigraft poly(L-lysine) by free solution capillary electrophoresis using polyelectrolyte multilayer coatings

Sébastien Roca, Laurent Leclercq, Herve Cottet

To cite this version:

Sébastien Roca, Laurent Leclercq, Herve Cottet. Size-based characterization of dendrigraft poly(L-lysine) by free solution capillary electrophoresis using polyelectrolyte multilayer coatings. Journal of Chromatography A, 2024, 1718, pp.464719. 10.1016/j.chroma.2024.464719 . hal-04560428

HAL Id: hal-04560428
https://hal.umontpellier.fr/hal-04560428v1

Size-based characterization of dendrigraft poly(L-lysine) by free solution capillary electrophoresis using polyelectrolyte multilayer coatings

Sébastien Roca[1], Laurent Leclercq[1*], Hervé Cottet[1*]

[1] IBMM, University of Montpellier, CNRS, ENSCM, Montpellier, France

[*] Corresponding authors: herve.cottet@umontpellier.fr ; laurent.leclercq@umontpellier.fr

Abstract

Dendrigraft poly(L-lysine) (DGL) constitutes a promising dendritic–like drug vehicle with high biocompatibility and straightforward access via ring-opening polymerization of N-carboxyanhydride in water. The characterization of the different generations of DGL is however challenging due to their heterogeneity in molar mass and branching ratio. In this work, free solution capillary electrophoresis was used to perform selective separation of the three first generations of DGL, and optimized conditions were developed to maximize inter-generation resolution. To reduce solute adsorption on the capillary wall, successive multiple ionic polymer layer (SMIL) coatings terminated with a polycation were deposited onto the inner wall surface. PEGylated polycation was also used as the last layer for the control of the electroosmotic flow (EOF), depending on the PEGylation degree and the methyl-polyethylene glycol (mPEG) chain length. 1 kDa mPEG chains and low grafting densities were found to be the best experimental conditions for a fine tuning of the EOF leading to high peak resolution. Molar mass polydispersity and polydispersity in effective electrophoretic mobility were successfully determined for the three first generations of DGL.

Keywords: Capillary electrophoresis, dendrigraft poly(L-lysine), polyelectrolyte multilayers, PEGylation, EOF modulation.

1. Introduction

Capillary electrophoresis (CE) is an analytical technique that presents numerous benefits for polymer and biopolymer analysis [1,2]. One limitation of the technique is analyte adsorption [1–6] that decrease the separation efficiency and the overall analysis performances and repeatability. Adsorption could be avoided or at least limited by the deposition of polyelectrolytes onto the capillary surface [7,8].

The implementation of Successive Multiple Ionic Polymer Layers (SMIL) capillary coating has demonstrated effective reduction of adsorption and improved analytical efficiency in protein analysis [9–23]. It was highlighted that the EOF remained consistently high when using fully ionized polyelectrolytes (EOF mobility typically around ± 40 Tiselius Units (TU), with 1 TU = 1×10^{-9} m^2 V^{-1} s^{-1}) [7]. This high EOF mobility resulted in short and repeatable analysis times but with possibly limited resolutions (R_s) due to fast analysis. Since EOF is primarily influenced by both the nature of the last polyelectrolyte layer and the composition of the background electrolyte (BGE) [21]. Modulating the EOF can be achieved by using a weak polyelectrolyte as the final layer and/or by changing the pH and ionic strength (I) of the BGE.

Due to its antifouling properties towards biological molecules [24–33], mPEG chains were chemically linked to different polycations, which were subsequently employed as top layers in SMIL capillary coatings [7]. It was demonstrated that the EOF was impacted when the mPEG chains length exceeded the Debye length, the latter depending on the BGE ionic strength. Competitions between the steric hindrance of mPEG chains and the shearing effect occurring in the Debbye length zone, resulted in a more or less pronounced hydrodynamic screening and decreased EOF value. The strong impact of mPEG chains density was highlighted in that study, with EOF value decreasing from -45 TU for non-PEGylated SMIL to only -5 TU for the same SMIL with the polycationic last layer modified with 5 kDa mPEG chains. Such neutral coating behavior allowed higher peak separation efficiency and better peak resolution (R_s) for protein separation [7].

A lot of applications can benefit from SMIL coatings and EOF modulation, especially (bio)polymer characterization and protein characterization by CE/MS [34–39]. PEGylated SMILs could pave the way to better CE-MS coupling, since high R_s and EOF control are key factors for efficient analysis. Too high EOF value disturbs the formation of stable electrospray droplets and may lead to ion suppression effects [40]. Various experiments concluded that near-zero EOF CE-MS experiments gave excellent peak resolution, separation efficiency and allowed wider detection window (leading to better mass spectra) [36–39].

In this work, we propose to use SMIL and PEGylated SMIL to characterize the three first generations of dendrigraft poly(L-lysine) (DGL). DGL polycations are synthesized by successive ring-opening polymerization of lysine protected N-carboxyanhydride in water, as described by Commeyras et al. [41]. The first DGL generation (G_1) gives linear α-poly(L-lysine) (α-PLL) oligomers. The second DGL generation (G_2) is a comb-like poly(L-lysine). The third generation of DGL (G3) is a hyperbranched poly-lysine. Up to five DGL generations can usually be synthesized, with increasing branching ratio and molar mass. Their high solubility in water [41], their high structural stability upon time [42], their easy chemical modification [43], their non-immunogenic behavior [44], their low cytotoxicity [45] and their biocompatibility [46] make DGL, and dendrimers of lysine in general, of great interest as novel drug delivery systems [47].

Regarding their size characterization, Dynamic Light Scattering (DLS) and Taylor Dispersion Analysis (TDA) were used to determine DGL hydrodynamic radius [48,49]. An almost linear correlation of the hydrodynamic radius with the generation number was observed, as expected for dendritic-like structures. The impact of organic solvent on R_h measurement was studied by Yevlampieva et al., revealing high flexibility of DGL structure, compared to other dendrimers [49]. Size-Exclusion Chromatography (SEC) coupled with multi-angle laser light scattering detection was used to determine the molar mass distribution and polydispersity indexes [41,50]. CE and TDA were successfully used to monitor surface functionalization of DGL [43]. DGL molar mass, hydrodynamic radius (R_h) and effective charge (z_{eff}) are presented in Table 1. Colorimetric methods were used to determine of the number of amino groups in DGL [48,51]. The overall DGL effective charge can be determined by capillary isotachophoresis, leading to information about counter-ion condensation which was found to dramatically increase with DGL generation number [52]. DGL characterization remains a complex task due to multiple distributions in molar mass and branching ratio, and the relative sample polydispersities.

Among the analytical targets, the inter-generation purity is a key point since DGL (as other dendritic structures) are synthesized step-by-step, from one generation to the other. Free solution CE analysis appears to be well-suited to check inter-generation DGL purity due to its simplicity, low-cost and relatively rapid and straightforward analysis without any sample preparation or filtration. The free solution electrophoretic mobility is known to be independent of the molar mass for linear polyelectrolytes above a certain molar mass (typically, 10^4 g/mol) [53], but depends on the branching ratio, notably because the effective charge of the dendrimer changes with the counter-ion condensation which is affected by the distance between adjacent charged monomers[52]. Collet et al. performed DGL analysis up to the fifth generation by CE using a fused silica capillary, with however incomplete separation between each generation [41]. G_1 analysis in free solution allows distinguishing seven peaks, with poor peak resolution. Capillary gel electrophoresis (CGE) allows the separation of G_1 oligomers, from 3 to 24 monomer units, but this method is more difficult to implement compared to free solution CE and is time-consuming.

In the present work, we aim to improve the free solution CE separation of DGL G_1 to G_3 using PEGylated SMIL and to determine their electrophoretic mobility dispersity and inter-generation purity.

2. Experimental section

2.1. Chemicals and Materials. Dendrigraft Poly(L-lysine) (DGL, G_1, G_2 and G_3) were synthesized in the laboratory according to [41]. 4-(2-hydroxyethyl)-1-piperazineethane sulfonic acid (HEPES, 99.5% purity), 2-Amino-2-(hydroxymethyl)-1,3-propanediol (Tris, > 99.9% purity), sodium nitrate (99.0% purity) and penta-Lysine (> 55% purity) were purchased from Sigma-Aldrich (Saint-Quentin-Fallavier, France). Sodium hydroxide (98 % purity) was purchased from Fluka (Saint-Quentin-Fallavier, France). Sodium azide (99.5% purity) was purchased from Merck (Darmstadt, Germany). Acetic acid (99.99% purity) was supplied by VWR Chemicals (Rosny-sous-Bois, France). Imidazole was purchased from Acros Organics (Geel, Belgium). Orthophosphoric acid (85% content) was purchased from Prolabo (Paris, France).

Methoxy-(polyethylene glycol)-succinimidyl carboxyl methyl ester (mPEG-NHS-SCM) of 1 kDa (PLS-215) and 5 kDa (PLS-213) average molar masses were purchased from Creative PEGWorks (Durham, NC, USA). Poly(allylamine hydrochloride) (PAH, M_w = 120-200 kDa) was supplied by Alfa Aesar (Kandel, Germany). Poly(diallyldimethylammonium chloride) (PDADMAC, M_w = 450 kDa) were purchased from Sigma Aldrich (Saint-Quentin-Fallavier, France). Poly(sodium styrenesulfonate) (PSS, M_w = 70 kDa) was purchased from Acros Organics (Geel, Belgium). Deionized water (18 MΩ.cm^{-1}) delivered by a Synergy UV water purification system (Millipore, Fontenay-sous-Bois, France) was used.

0.1 µm cut□off Durapore membrane filters were purchased from Millipore (Molsheim, France). Dialysis tubings (cut-off: 1, 3.5, 8 and 12–14 kDa) were purchased from Spectrum Labs (San Francisco, CA, USA).

PAH were PEGylated with either 1 kDA mPEG or 5 kDa mPEG, following EDC/NHS synthesis protocol, as described in a previous paper [7]. For the 5 kDa mPEG polyelectrolyte modification, lower grafting ratio than the targeted one was found due to possible steric hindrance of the long mPEG chains. In contrast, a better control of the grafting ratio was obtained in the case of 1 kDa mPEGylation. PEGylated PAH polycations were characterized by ^{1}H NMR (as given in supporting information in Figure SI1 and SI2) and SEC-MALLS (Figure SI3). The main characteristics are gathered in Table 2. More details about the experimental conditions for the characterization can be found in ref [7]. PEGylated PAH were named PAH-g-$(mPEG_x)_y$, where x corresponds to the mPEG length and y to the measured PEGylated grafted ratio.

2.2. SMIL coatings. All SMIL capillary coatings were composed of a 4-layer $(PDADMAC/PSS)_2$ substructure terminated with either native or PEGylated PAH and were named $(PDADMAC/PSS)_2$-$(PAH\text{-}g\text{-}(mPEG_x)_y)_1$. Capillary coating procedure was performed according to [7,8,54]: flush at 930 mbar with NaOH 1 M solution for 10 min, followed by 5 min with pure water and 10 min with construction buffer (HEPES/NaOH, 20 mM / 10 mM, pH 7.4). Next, polyelectrolyte solution (3 gL^{-1} of

PDADMAC or PSS in construction buffer) was flushed for 7 min, followed by a capillary rinsing with the construction buffer (3 min). This step was repeated four times, starting with PDADMAC. For the fifth layer coating, polyelectrolyte solution consisted of PAH (or its PEGylated derivative) dissolved at 3 gL^{-1} in the construction buffer, followed by a 3 min rinsing step with HEPES solution and 5 min wait. Finally, the coated capillary was flushed with BGE for 10 min.

2.3. Separation of dendrigraft poly(L-lysine) by capillary zone electrophoresis in free solution. Capillary zone electrophoresis experiments were performed on an Agilent 7100 CE piloted by ChemStation software, using 58.5 or 88.5 cm capillary (50 and 80 cm of effective length, respectively, 50 µm capillary I.D. and 359 µm capillary O.D.) and 125/250 mM Tris-phosphate BGE, pH 2.2 (I = 134.7 mM). Analyte (DGL G_1, G_2 and G_3) were kept separately in BGE (at 2 gL^{-1}) in the freezer. BGE was flushed for 3 min at 1 bar between each run. The separation voltage was +20 kV. DMF (0.001% m/v in the BGE) and imidazole (0.001% m/v in BGE) were hydrodynamically injected as markers for 3 s at 30 mbar, followed by injection of DGL (2 or 0.5 gL^{-1} each in the BGE) for 4 s at 30 mbar. The temperature of the cartridge was set at 25°C. Detection wavelengths were 214 and 200 nm.

2.4. Polydispersity index (PDI) measurement. Polydispersity index (*PDI*) gives information about the dispersion of a given polymer distribution. *PDI* can be determined on molar mass distribution using SEC, on hydrodynamic radius distribution using TDA or DLS [41], or on electrophoretic mobility distribution using CE [55]. As described by Burchard in 1999 [56], polydispersity index relative to the mass size distribution (PDI_M) can be expressed as (eq. 1):

$$PDI_M = \frac{M_w}{M_n} \tag{1}$$

where M_n and M_w are the number and weight average molar mass of the analyte, respectively. Polydispersity index relative to the effective electrophoretic mobility distribution (PDI_μ) can be expressed as (eq. 2) [56,57] :

$$PDI_\mu = \frac{\sigma_\mu^2}{\bar{\mu}_w^2} \tag{2}$$

with σ_{μ}^2 being the peak variance of the electropherogram modified by turning time x-scale into effective electrophoretic mobility x-scale [58] and $\bar{\mu}_w^2$ being the average effective electrophoretic mobility of the analyte.

3. Results and discussion

3.1. Improving linear poly(L-lysine) oligomers separation in free solution CE by EOF modulation.

In the first part of this work, we aimed to determine the best experimental conditions for the analysis of the first generation of dendrigraft poly(L-lysine) (G_1) in free solution CE. G_1 is a linear oligomeric poly(L-lysine). Experiments were carried out using Tris-phosphate buffer (125 mM / 250 mM, pH 2.2) as background electrolyte (BGE) and a 50 µm I.D. (O.D. = 359 µm) fused silica capillary of 58.5 cm long (50 cm to the detector). Imidazole was used as the mobility marker. Effective electrophoretic mobility of imidazole was +37.0 TU at +20 kV. In free solution CE, the electrophoretic mobility of short oligomers can vary due to hydrodynamic coupling [59,60], but the main cause of the selectivity in the present case is due to specific interaction between phosphate ions ($H_2PO_4^-$) and poly-L-lysine [61,62].

As shown in Figure 1, the CE analysis of G_1 in a bare fused silica capillary at +20kV led to the detection of broad distribution with low resolution between oligomers. The apparent mobility with the fused silica capillary is +5.56 ± 0.06 TU. The adsorption of poly(L-Lysine) onto the capillary wall is limited in phosphate buffer at pH 2.2 due to almost neutral silica surface and probable interactions of phosphate ions with poly(L-lysine) [62].

To improve this separation in free solution (i.e. without addition of gel or entangled polymer solution in the BGE), it is possible to reduce the EOF magnitude, or even to reverse the EOF in a controlled manner. By this way, the apparent mobility of the G_1 oligomers is decreased, which consequently increases the apparent selectivity, and thus, the resolution, to the detriment of the analysis time. As for G_1 separation, it is worth noting that the free solution electrophoretic effective mobility of the poly(L-lysine) oligomers is changing with the molar mass due to two effects: interaction of oligolysines with hydrogenophosphate ions and to a lower extent due to relaxation effect [62].

To improve G_1 separation, we used a 5-layers SMIL coating based on poly(diallyldimethylammonium chloride) (PDADMAC) as the polycation, sodium poly(styrene sulfonate) (PSS) as the polyanion, and a last layer containing variously PEGylated polyallylamine hydrochloride PAH-g-$(\text{mPEG})_x$ (where x is the molar proportion of PEGylation on the PAH). 1 kDa and 5 kDa mPEG were used as grafting agents. Synthesis and characterization of PEGylated PAH were realized following the protocol previously described by Roca et al.[7]. As shown in Figure 1, 5kDa mPEG slightly reduces the EOF compared to fused silica but do not reverse the EOF direction. This is due to the fact that the 5kDa mPEG chain length (hydrodynamic diameter ~ 3.5 nm calculated from Mark-Houwink coefficients) [63] is much higher than the Debye length (0.83 nm in the Tris-phosphate BGE), leading to important hydrodynamic screening in the electrical double layer of the EOF generated by the cationic charges. Therefore, SMIL terminated with a PAH-g-$(\text{mPEG}_{5\text{kDa}})_x$ led to close to zero EOF, as displayed in Figure 2. The best EOF regulation was obtained using PAH-g-$(\text{mPEG}_{1\text{kDa}})_x$, leading to a broad range of EOF mobility from -1.01 ± 0.11 TU for the 23.5% 1 kDa PEGylated PAH to -16.68 ± 0.10 TU in the case of unmodified PAH. EOF mobility could be successfully regulated according to the 1 kDa mPEG proportion. A total of 10 peaks were detected for G_1 in about 20 min using SMIL coating terminated with PAH-g-$(\text{mPEG}_{1\text{kDa}})_{0.065}$ as the last layer. As for the G1 separation, the unPEGylated PAH gives even higher resolution with an analysis time of about 35 min.

3.2. Optimize the separation of the three first generations of DGL. EOF regulation was applied to the analysis of DGL G_1, G_2 and G_3 in free solution. This inter-generation separation is essential to quantify the inter-generation purity. The separation between DGL generations is notably driven by the drop in the effective charge per monomer with increasing generation number [52] which can be explained by higher counter-ion condensation for higher branching ratios. The DGL concentration was reduced from 2 gL^{-1} to 0.5 gL^{-1} to limit the electromigration dispersion (overloading effect) and UV-detection was set at 200 nm for better sensitivity. G_1, G_2 and G_3 were injected separately to better visualize the co-migrations between DGL generations. As shown in Figure 3A, using a 58.5 cm long bare fused silica capillary, G_1 to G_3 DGL were detected in less than 10 min with only partial separation between generations, and only 4 peaks that can be distinguished for G_1 oligomers. Using

PAH-g-$(mPEG_{1kDa})_{0.133}$ as the last layer gave better results with 7 distinguishable peaks for G_1 and better separation between G_1 and G_2 and between G_2 and G_3. Finally, PAH-g-$(mPEG_{1kDa})_{0.065}$ as the last layer afforded the highest peak resolution, with 13 peaks detected for G_1 and improved peak separation between G_1 and G_2. The three DGL generations were detected in 35 min (Figure 3A, upper trace). UnPEGylated PAH was not used due to too high migration times.

Similar experiments were carried out on an 88.5 cm long capillary (80 cm to the detector) to further increase the peak resolution (Figure 3B). 13 different peaks were detected using 13.3% and 6.5% PEGylated PAH as last layer, with 2.38 and 2.53 peak resolution between the two highest peaks of G_1 (corresponding to a polymerization degree (*DP*) = 6 and 7), respectively, while other experiments presented in Figure 3 never exceeded peak resolution of 1.50 (see Table SI1). 88.5 cm long capillaries were used to determine inter-generation DGL purity.

3.3. Characterization of DGL polydispersity and inter-generational purity.

Peak assignment of G_1 was performed on a 58.5 cm long fused silica capillary, coated with $(PDADMAC/PSS)_2$-(PAH-g-$(mPEG_{1kDa})_{0.033})_1$. As shown in Figure 4, 13 peaks were detected in 26 min. The peak assignment was done by spiking the G_1 sample with pentalysine (see Figure SI4).

Polydispersity index (*PDI*) of all three generations were calculated from the experimental data obtained with an 88.5 cm long fused silica capillary, coated with $(PDADMAC/PSS)_2$-(PAH-g-$(mPEG_{1kDa})_{0.065})_1$ SMIL. For G_1, *PDI* was measured according to two different ways, i.e. in terms of molar mass polydispersity (PDI_M) and in terms of electrophoretic effective mobility polydispersity (PDI_μ). Equations used to determine PDI_M and PDI_μ are given in section 2.3. The determination of PDI_μ requires the transformation of the raw electropherogram (absorbance $A(t)$ *vs* migration time (t)) into effective electrophoretic mobility distribution ($P(\mu) \sim A(t) \times t$, see Figure 5A), following previously described protocols [58]. More details about these transformations are provided in supporting information (Figure SI5 and SI6). Both *PDI* values demonstrated relatively low polydispersity (Table 3).

In the case of G_2 and G_3, PDI_M could not be determined since it is not possible to get the molar mass (or DP) distributions. Indeed, to get the molar mass distributions, a bijective function between the effective mobility and the molar mass would be required. Since the electrophoretic mobility of the hyperbranched dendrimers are depending in a complex manner with the branching ratio, the effective charge and indirectly with the molar mass, it is not possible to get such bijective function. In other words, a given effective mobility can correspond to two (or more) DGL structures having different branching ratios and different molar masses. Higher branching ratios are strongly lowering the effective charge per monomer due to stronger counter-ion condensation [52].This explains why the DGL effective mobility decreased with DGL generation (higher branching ratio and lower effective charge per monomer). Only PDI_μ values were calculated for G_2 and G_3 (Table 3). Since both G_2 and G_3 presented some intergenerational impurities (G_1 in G_2 sample and both G_1 and G_2 in G_3 sample), PDI_μ was estimated on the main peak (see Figure 5B and 5C). PDI_μ value decreased with increasing the generation number. Beyond inter generation comparisons, PDI are of interest for the synthetic chemist to compare the batch-to-batch reproducibility.

The inter-generational purity was calculated for G_2 and G_3, using a $(PDADMAC/PSS)_2$-$(PAH$-g-$(mPEG_{1kDa})_{0.065})_1$ coated capillary (Figure 6). Using CE-Val software to measure time-corrected peak area, residual G_1 in G_2 was found to be about 4.3 ± 1.4 %, corresponding to 25 mgL^{-1} concentration of G_1 in G_2. The same way, residual G_1 and G_2 in G_3 were found to be about 56 mgL^{-1} (6.6 ± 1.0 %) and 97 mgL^{-1} (13.2 ± 2.8 %), respectively. The error bars given for the inter-generational purities were evaluated based on the visual evaluation of the integration limits, as depicted by the red arrows in Figure 6.

Conclusion

In this paper, capillary coatings based on successive multiple ionic polymer layers (SMIL) terminated with a PEGylated PAH layer were used to characterize the polydispersity and the inter-generation purity of three dendrigraft poly(L-lysine)s generations. By changing the proportion of PEGylation a controlled regulation of the EOF could be obtained to improve the intergeneration separation. 13.3%, 6.5% and 3.3% 1kDa PEGylated polycations led to better resolution compared to bare fused silica capillary. Finally, polydispersity indexes in mass and mobility were determined after adequate transformations of the electropherograms into effective mobility distribution or *DP* distributions.

References

[1] L. Leclercq, M. Morvan, J. Koch, C. Neusüß, H. Cottet, Modulation of the electroosmotic mobility using polyelectrolyte multilayer coatings for protein analysis by capillary electrophoresis, Analytica Chimica Acta 1057 (2019) 152–161. https://doi.org/10.1016/j.aca.2019.01.008.

[2] M.G. Khaledi, High-Performance Capillary Electrophoresis Theory, Techniques, and Applications, 1998.

[3] M.R. Schure, A.M. Lenhoff, Consequences of wall adsorption in capillary electrophoresis: theory and simulation, Anal. Chem. 65 (1993) 3024–3037. https://doi.org/10.1021/ac00069a015.

[4] S. Ghosal, Fluid mechanics of electroosmotic flow and its effect on band broadening in capillary electrophoresis, Electrophoresis 25 (2004) 214–228. https://doi.org/10.1002/elps.200305745.

[5] S. Ghosal, Electrokinetic flow and dispersion in capillary electrophoresis, Annu. Rev. Fluid Mech. 38 (2006) 309–338. https://doi.org/10.1146/annurev.fluid.38.050304.092053.

[6] B. Gaš, M. Štědrý, E. Kenndler, Peak broadening in capillary zone electrophoresis, Electrophoresis 18 (1997) 2123–2133. https://doi.org/10.1002/elps.1150181203.

[7] S. Roca, L. Leclercq, P. Gonzalez, L. Dhellemmes, L. Boiteau, G. Rydzek, H. Cottet, Modifying last layer in polyelectrolyte multilayer coatings for capillary electrophoresis of proteins, J. Chromatogr. A 1692 (2023) 463837. https://doi.org/10.1016/j.chroma.2023.463837.

[8] L. Dhellemmes, L. Leclercq, A. Höchsmann, C. Neusüß, J.-P. Biron, S. Roca, H. Cottet, Critical parameters for highly efficient and reproducible polyelectrolyte multilayer coatings for protein separation by capillary electrophoresis, J. Chromatogr. A 1695 (2023) 463912. https://doi.org/10.1016/j.chroma.2023.463912.

[9] L. Leclercq, C. Renard, M. Martin, H. Cottet, Quantification of adsorption and optimization of separation of proteins in capillary electrophoresis, Anal. Chem. 92 (2020) 10743–10750. https://doi.org/10.1021/acs.analchem.0c02012.

[10] L. Hajba, A. Guttman, Continuous-flow-based microfluidic systems for therapeutic monoclonal antibody production and organ-on-a-chip drug testing, J. Flow Chem. 7 (2017) 118–123. https://doi.org/10.1556/1846.2017.00014.

[11] V. Dolník, Capillary electrophoresis of proteins 2005–2007, Electrophoresis 29 (2008) 143–156. https://doi.org/10.1002/elps.200700584.

[12] P.G. Righetti, C. Gelfi, B. Verzola, L. Castelletti, The state of the art of dynamic coatings, Electrophoresis 22 (2001) 603–611. https://doi.org/10.1002/1522-2683(200102)22:4<603::AID-ELPS603>3.0.CO;2-N.

[13] C.A. Lucy, A.M. MacDonald, M.D. Gulcev, Non-covalent capillary coatings for protein separations in capillary electrophoresis, J. Chromatogr A 1184 (2008) 81–105. https://doi.org/10.1016/j.chroma.2007.10.114.

[14] K.S. McMillan, A.G. McCluskey, A. Sorensen, M. Boyd, M. Zagnoni, Emulsion technologies for multicellular tumour spheroid radiation assays, Analyst 141 (2016) 100–110. https://doi.org/10.1039/C5AN01382H.

[15] S. Štěpánová, V. Kašička, Recent applications of capillary electromigration methods to separation and analysis of proteins, Analytica Chimica Acta 933 (2016) 23–42. https://doi.org/10.1016/j.aca.2016.06.006.

[16] S. Štěpánová, V. Kašička, Applications of capillary electromigration methods for separation and analysis of proteins (2017–mid 2021) – A review, Analytica Chimica Acta 1209 (2022) 339447. https://doi.org/10.1016/j.aca.2022.339447.

[17] S. Bekri, L. Leclercq, H. Cottet, Polyelectrolyte multilayer coatings for the separation of proteins by capillary electrophoresis: Influence of polyelectrolyte nature and multilayer crosslinking, J. Chromatogr. A 1399 (2015) 80–87. https://doi.org/10.1016/j.chroma.2015.04.033.

[18] A. Pallotta, I. Clarot, J. Beurton, B. Creusot, T. Chaigneau, A. Tu, P. Lavalle, A. Boudier, Analytical strategy for studying the formation and stability of multilayered films containing gold nanoparticles, Anal. Bioanal. Chem. 413 (2021) 1473–1483. https://doi.org/10.1007/s00216-020-03113-6.

[19] L. Villemet, A. Cuchet, C. Desvignes, C.E. Sänger–van de Griend, Protein mapping of peanut extract with capillary electrophoresis, Electrophoresis 43 (2022) 1027–1034. https://doi.org/10.1002/elps.202100004.

[20] M. Horká, J. Šalplachta, P. Karásek, M. Roth, Sensitive identification of milk protein allergens using on-line combination of transient isotachophoresis/micellar electrokinetic chromatography and capillary isoelectric focusing in fused silica capillary with roughened part, Food Chem. 377 (2022) 131986. https://doi.org/10.1016/j.foodchem.2021.131986.

[21] R. Konášová, M. Butnariu, V. Šolínová, V. Kašička, D. Koval, Covalent cationic copolymer coatings allowing tunable electroosmotic flow for optimization of capillary electrophoretic separations, Analytica Chimica Acta 1178 (2021) 338789. https://doi.org/10.1016/j.aca.2021.338789.

[22] V. Šolínová, P. Tůma, M. Butnariu, V. Kašička, D. Koval, Covalent anionic copolymer coatings with tunable electroosmotic flow for optimization of capillary electrophoretic separations, Electrophoresis 43 (2022) 1953–1962. https://doi.org/10.1002/elps.202200130.

[23] G.W. Somsen, R. Haselberg, K. Michalikova, E. Domínguez-Vega, Middle-Up Characterization of the monoclonal antibody infliximab by capillary zone electrophoresis–mass spectrometry, LCGC Europe-03-01-2019, Volume 32, Issue 3 (2019).

[24] M. Hedayati, D.F. Marruecos, D. Krapf, J.L. Kaar, M.J. Kipper, Protein adsorption measurements on low fouling and ultralow fouling surfaces: A critical comparison of surface characterization techniques, Acta Biomaterialia 102 (2020) 169–180. https://doi.org/10.1016/j.actbio.2019.11.019.

[25] C.-M. Xing, F.-N. Meng, M. Quan, K. Ding, Y. Dang, Y.-K. Gong, Quantitative fabrication, performance optimization and comparison of PEG and zwitterionic polymer antifouling coatings, Acta Biomaterialia 59 (2017) 129–138. https://doi.org/10.1016/j.actbio.2017.06.034.

[26] C. Zhang, J. Yuan, J. Lu, Y. Hou, W. Xiong, H. Lu, From neutral to zwitterionic poly(α-amino acid) nonfouling surfaces: Effects of helical conformation and anchoring orientation, Biomater. 178 (2018) 728–737. https://doi.org/10.1016/j.biomaterials.2018.01.052.

[27] B.L. Leigh, E. Cheng, L. Xu, A. Derk, M.R. Hansen, C.A. Guymon, Antifouling photograftable zwitterionic coatings on PDMS substrates, Langmuir 35 (2019) 1100–1110. https://doi.org/10.1021/acs.langmuir.8b00838.

[28] X. Lin, P. Jain, K. Wu, D. Hong, H.-C. Hung, M.B. O’Kelly, B. Li, P. Zhang, Z. Yuan, S. Jiang, Ultralow fouling and functionalizable surface chemistry based on zwitterionic carboxybetaine random copolymers, Langmuir 35 (2019) 1544–1551. https://doi.org/10.1021/acs.langmuir.8b02540.

[29] R.J. Smith, M.G. Moule, P. Sule, T. Smith, J.D. Cirillo, J.C. Grunlan, Polyelectrolyte Multilayer Nanocoating Dramatically Reduces Bacterial Adhesion to Polyester Fabric, ACS Biomater. Sci. Eng. 3 (2017) 1845–1852. https://doi.org/10.1021/acsbiomaterials.7b00250.

[30] F. Boulmedais, B. Frisch, O. Etienne, P. Lavalle, C. Picart, J. Ogier, J.-C. Voegel, P. Schaaf, C. Egles, Polyelectrolyte multilayer films with pegylated polypeptides as a new type of anti-microbial protection for biomaterials, Biomater. 25 (2004) 2003–2011. https://doi.org/10.1016/j.biomaterials.2003.08.039.

[31] Z. Zhang, M. Moxey, A. Alswieleh, A.J. Morse, A.L. Lewis, M. Geoghegan, G.J. Leggett, Effect of salt on phosphorylcholine-based zwitterionic polymer brushes, Langmuir 32 (2016) 5048–5057. https://doi.org/10.1021/acs.langmuir.6b00763.

[32] C. Wang, G.K. Such, A. Widjaya, H. Lomas, G. Stevens, F. Caruso, S.E. Kentish, Click poly(ethylene glycol) multilayers on RO membranes: Fouling reduction and membrane characterization, J. Membrane Sci. 409–410 (2012) 9–15. https://doi.org/10.1016/j.memsci.2012.02.049.

[33] W.-L. Chen, R. Cordero, H. Tran, C.K. Ober, *50th Anniversary Perspective* : Polymer Brushes: Novel Surfaces for Future Materials, Macromolecules 50 (2017) 4089–4113. https://doi.org/10.1021/acs.macromol.7b00450.

[34] F.P. Gomes, J.R. Yates, Recent trends of capillary electrophoresis- mass spectrometry in proteomics research, Mass Spec. Rev. 38 (2019) 445–460. https://doi.org/10.1002/mas.21599.

[35] M. Pattky, C. Huhn, Advantages and limitations of a new cationic coating inducing a slow electroosmotic flow for CE-MS peptide analysis: a comparative study with commercial coatings, Anal. Bioanal. Chem. 405 (2013) 225–237. https://doi.org/10.1007/s00216-012-6459-8.

[36] Y. Zhao, L. Sun, M.D. Knierman, N.J. Dovichi, Fast separation and analysis of reduced monoclonal antibodies with capillary zone electrophoresis coupled to mass spectrometry, Talanta 148 (2016) 529–533. https://doi.org/10.1016/j.talanta.2015.11.020.

[37] R. Haselberg, T. De Vijlder, R. Heukers, M.J. Smit, E.P. Romijn, G.W. Somsen, E. Domínguez-Vega, Heterogeneity assessment of antibody-derived therapeutics at the intact and middle-up level by low-flow sheathless capillary electrophoresis-mass spectrometry, Analytica Chimica Acta 1044 (2018) 181–190. https://doi.org/10.1016/j.aca.2018.08.024.

[38] M. Han, B.M. Rock, J.T. Pearson, D.A. Rock, Intact mass analysis of monoclonal antibodies by capillary electrophoresis—mass spectrometry, J. Chromatogr. B 1011 (2016) 24–32. https://doi.org/10.1016/j.jchromb.2015.12.045.

[39] R. Haselberg, G.J. De Jong, G.W. Somsen, Low-flow sheathless capillary electrophoresis–mass spectrometry for sensitive glycoform profiling of intact pharmaceutical proteins, Anal. Chem. 85 (2013) 2289–2296. https://doi.org/10.1021/ac303158f.

[40] G. Jarvas, B. Fonslow, A. Guttman, Ionization efficiency, ion suppression and detection sensitivity of CESI-MS, https://sciex.com/tech-notes/ce/ionization-efficiency--ion-suppression-and-detection-sensitivity.

[41] H. Collet, E. Souaid, H. Cottet, A. Deratani, L. Boiteau, G. Dessalces, J.-C. Rossi, A. Commeyras, R. Pascal, An expeditious multigram-scale synthesis of lysine dendrigraft (DGL) polymers by aqueous *N* -carboxyanhydride polycondensation, Chem. Eur. J. 16 (2010) 2309–2316. https://doi.org/10.1002/chem.200901734.

[42] G. Coussot, T. Moreau, C. Faye, F. Vigier, M. Baqué, A. Le Postollec, S. Incerti, M. Dobrijevic, O. Vandenabeele-Trambouze, Biochip-based instruments development for space exploration: influence of the antibody immobilization process on the biochip resistance to freeze-drying, temperature shifts and cosmic radiations, Int. J. Astrobiol. 16 (2017) 190–199. https://doi.org/10.1017/S1473550416000173.

[43] T. Liu, F. Oukacine, H. Collet, A. Commeyras, L. Vial, H. Cottet, Monitoring surface functionalization of dendrigraft poly-L-lysines via click chemistry by capillary electrophoresis and Taylor dispersion analysis, J. Chromatogr. A 1273 (2013) 111–116. https://doi.org/10.1016/j.chroma.2012.11.074.

[44] B. Romestand, J.-L. Rolland, A. Commeyras, G. Coussot, I. Desvignes, R. Pascal, O. Vandenabeele-Trambouze, Dendrigraft poly- L -lysine: A non-immunogenic synthetic carrier for antibody production, Biomacromolecules 11 (2010) 1169–1173. https://doi.org/10.1021/bm9012056.

[45] J. Hofman, M. Buncek, R. Haluza, L. Streinz, M. Ledvina, P. Cigler, In vitro transfection mediated by dendrigraft poly(L -lysines): The effect of structure and molecule size, Macromol. Biosci. 13 (2013) 167–176. https://doi.org/10.1002/mabi.201200303.

[46] J. Chamieh, J.P. Biron, L. Cipelletti, H. Cottet, Monitoring biopolymer degradation by Taylor dispersion analysis, Biomacromolecules 16 (2015) 3945–3951. https://doi.org/10.1021/acs.biomac.5b01260.

[47] J.-P. Francoia, L. Vial, Everything you always wanted to know about poly- L -lysine dendrigrafts (but were afraid to ask), Chem. Eur. J. 24 (2018) 2806–2814. https://doi.org/10.1002/chem.201704147.

[48] H. Cottet, M. Martin, A. Papillaud, E. Souaïd, H. Collet, A. Commeyras, Determination of dendrigraft poly- L -Lysine diffusion coefficients by Taylor dispersion analysis, Biomacromolecules 8 (2007) 3235–3243. https://doi.org/10.1021/bm070268j.

[49] N. Yevlampieva, A. Dobrodumov, O. Nazarova, O. Okatova, H. Cottet, Hydrodynamic behavior of dendrigraft polylysines in water and dimethylformamide, polymers 4 (2012) 20–31. https://doi.org/10.3390/polym4010020.

[50] B. Maret, A. Crépet, C. Faye, L. Garrelly, C. Ladavière, Molar-mass analysis of dendrigraft poly(L -lysine) (DGL) polyelectrolytes by SEC-MALLS: The “Cornerstone” refractive index increment, Macromol. Chem. Phys. 216 (2015) 95–105. https://doi.org/10.1002/macp.201400400.

[51] G. Coussot, E. Nicol, A. Commeyras, I. Desvignes, R. Pascal, O. Vandenabeele-Trambouze, Colorimetric quantification of amino groups in linear and dendritic structures, Polym. Int. 58 (2009) 511–518. https://doi.org/10.1002/pi.2560.

[52] A. Ibrahim, D. Koval, V. Kašička, C. Faye, H. Cottet, Effective charge determination of dendrigraft poly- L -lysine by capillary isotachophoresis, Macromolecules 46 (2013) 533–540. https://doi.org/10.1021/ma302125f.

[53] H. Cottet, P. Gareil, O. Theodoly, C.E. Williams, A semi-empirical approach to the modeling of the electrophoretic mobility in free solution: Application to polystyrenesulfonates of various sulfonation rates, Electrophoresis 21 (2000) 3529–3540. https://doi.org/10.1002/1522-2683(200011)21:17<3529::AID-ELPS3529>3.0.CO;2-2.

[54] S. Roca, L. Dhellemmes, L. Leclercq, Polyelectrolyte multilayers in capillary electrophoresis, ChemPlusChem 87 (2022). https://doi.org/10.1002/cplu.202200028.

[55] J.J. Thevarajah, A.T. Sutton, A.R. Maniego, E.G. Whitty, S. Harrisson, H. Cottet, P. Castignolles, M. Gaborieau, Quantifying the heterogeneity of chemical structures in complex charged polymers through the dispersity of their distributions of electrophoretic mobilities or of compositions, Anal. Chem. 88 (2016) 1674–1681. https://doi.org/10.1021/acs.analchem.5b03672.

[56] W. Burchard, Solution Properties of Branched Macromolecules, in: J. Roovers (Ed.), Branched Polymers II, Springer Berlin Heidelberg, Berlin, Heidelberg, 1999: pp. 113–194. https://doi.org/10.1007/3-540-49780-3_3.

[57] I. Desvignes, J. Chamieh, H. Cottet, Separation and characterization of highly charged polyelectrolytes using free-solution capillary electrophoresis, Polymers 10 (2018) 1331. https://doi.org/10.3390/polym10121331.

[58] J. Chamieh, M. Martin, H. Cottet, Quantitative Analysis in Capillary Electrophoresis: Transformation of Raw Electropherograms into Continuous Distributions, Anal. Chem. 87 (2015) 1050–1057. https://doi.org/10.1021/ac503789s.

[59] H. Cottet, P. Gareil, From small charged molecules to oligomers: A semiempirical approach to the modeling of actual mobility in free solution, Electrophoresis 21 (2000) 1493–1504. https://doi.org/10.1002/(SICI)1522-2683(20000501)21:8<1493::AID-ELPS1493>3.0.CO;2-E.

[60] K. Grass, U. Böhme, U. Scheler, H. Cottet, C. Holm, Importance of hydrodynamic shielding for the dynamic behavior of short polyelectrolyte chains, Phys. Rev. Lett. 100 (2008) 096104. https://doi.org/10.1103/PhysRevLett.100.096104.

[61] S.A. Allison, C. Perrin, H. Cottet, Modeling the electrophoresis of oligolysines, Electrophoresis 32 (2011) 2788–2796. https://doi.org/10.1002/elps.201100006.

[62] H. Wu, S.A. Allison, C. Perrin, H. Cottet, Modeling the electrophoresis of highly charged peptides: Application to oligolysines, J. Sep. Sci. 35 (2012) 556–562. https://doi.org/10.1002/jssc.201100873.

[63] E.A. Bekturov, Z.K. Bakauova, Synthetic Water-soluble Polymers in Solution: Polymeric Acids Anf Their Salts - Cationic Polyelectrolytes - Non-ionic Water-soluble Polymers - Water-soluble Polymers, Basel Heidelberg, 1986.

LIST OF CAPTIONS

Figure 1 : Impact of the capillary coating on DGL G_1 analysis by CE in free solution. Experimental conditions: fused silica capillary of 58.5 cm total length (50 cm to detector) × 50 µm I.D. (359 µm O.D.). Coating: none (fused silica) or $(PDADMAC/PSS)_2$ + a last layer as indicated in the figure. Coating protocol: See section 2.1. BGE: Tris-phosphate buffer (125 / 250 mM), pH 2.2. Applied voltage: +20 kV. Hydrodynamic injection: 30 mbar, 4 s (0.27% of total capillary volume). Concentration of analytes: I: Imidazole (0.001% m/v) used as mobility marker, G_1: DGL G_1 (2 gL^{-1} in BGE). Temperature: 25°C. UV detection: 214 nm.

Figure 2 : Impact of the proportion of mPEG in the last layer of a 5 layers SMIL coating on electroosmotic mobility. Same experimental conditions as in Figure 1. Error bars were estimated as ± one SD on $n = 5$ repetitions.

Figure 3: Impact of the capillary coating for the separation of DGL G_1, G_2 and G_3 at pH 2.2 on a 58.5 cm (A) and 88.5 cm (B) long capillary by free solution CE. Experimental conditions: fused silica capillary of 58.5 and 88.5 cm total length (50 and 80 cm to detector) × 50 µm I.D. (359 µm O.D.). Coating: none (fused silica) or $(PDADMAC/PSS)_2$ + last layer as indicated in the figure. Coating protocol: See section 2.1. BGE: Tris-phosphate buffer (125 / 250 mM), pH 2.2. Applied voltage: +20 kV. Hydrodynamic injection: 30 mbar, 4 s (0.27% and 0.13% of total capillary volume, respectively). Concentration of analytes: I: Imidazole (0.001% m/v) used as mobility marker, G_1: DGL G_1 (0.5 gL^{-1}), G_2: DGL G_2 (0.5 gL^{-1}) and G_3: DGL G_3 (0.5 gL^{-1}) all in BGE. Temperature: 25°C. UV detection: 200 nm.

Figure 4: Optimized DGL G_1 analysis at pH 2.2 using $(PDADMAC/PSS)_2$-(PAH-g-$(mPEG_{1kDa})_{0.033})_1$ coated capillary by free solution CE. Experimental conditions: fused silica capillary of 58.5 total length (50 cm to detector) × 50 µm I.D. (359 µm O.D.). Coating protocol: See section 2.1. BGE: Tris-phosphate buffer (125 / 250 mM), pH 2.2 Applied voltage: + 20 kV. Hydrodynamic injection: 30 mbar, 4 s (0.27% of total capillary volume). Concentration of analytes: G_1: DGL G_1 (0.5 gL^{-1} in BGE). Temperature: 25°C. UV detection: 200 nm.

Figure 5: Determination of PDI_M-1 and PDI_μ for G_1 (A), G_2 (B) and G_3 (C) using $(PDADMAC/PSS)_2$-(PAH-g-$(mPEG_{1kDa})_{0.065})_1$ coated capillary by CE in free solution. Experimental conditions: fused silica capillary of 88.5 total length (80 cm to detector) × 50 µm I.D. (359 µm O.D.). Coating protocol: See section 2.1. BGE: Tris-phosphate buffer (125 / 250 mM), pH 2.2 Applied voltage: + 20 kV. Hydrodynamic injection: 30 mbar, 4 s (0.13% of total capillary volume). Concentration of analytes: DGL G_1, G_2 and G_3 (0.5 gL^{-1} in BGE). Temperature: 25°C. UV detection: 200 nm.

Figure 6 : Determination of intergenerational impurity for G_2 and G_3 using $(PDADMAC/PSS)_2$-(PAH-g-$(mPEG_{1kDa})_{0.065})_1$ coated capillary by CE in free solution. Same experimental conditions as in Figure 5. Baseline and integration limits used for intergeneration purity are displayed in the figure. The middle ticks display the limits used to determine the average values given in the text. The red arrows depict the integration limits used to estimate the errors on the inter-generation purities.

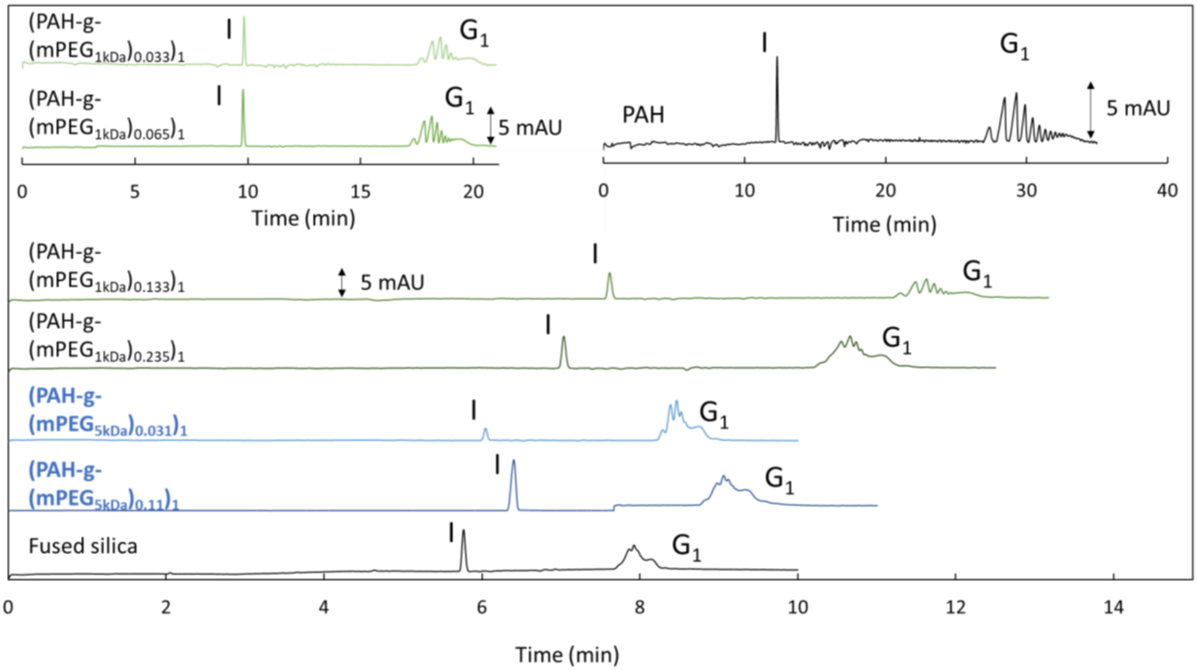
(PAH-g-(mPEG$_{1kDa}$)$_{0.033}$)$_1$
I
G$_1$
(PAH-g-(mPEG$_{1kDa}$)$_{0.065}$)$_1$
I
G$_1$
5 mAU
0
5
10
15
20
Time (min)
PAH
I
G$_1$
5 mAU
0
10
20
30
40
Time (min)
(PAH-g-(mPEG$_{1kDa}$)$_{0.133}$)$_1$
5 mAU
I
G$_1$
(PAH-g-(mPEG$_{1kDa}$)$_{0.235}$)$_1$
I
G$_1$
(PAH-g-(mPEG$_{5kDa}$)$_{0.031}$)$_1$
I
G$_1$
(PAH-g-(mPEG$_{5kDa}$)$_{0.11}$)$_1$
I
G$_1$
Fused silica
I
G$_1$
0
2
4
6
8
10
12
14
Time (min)

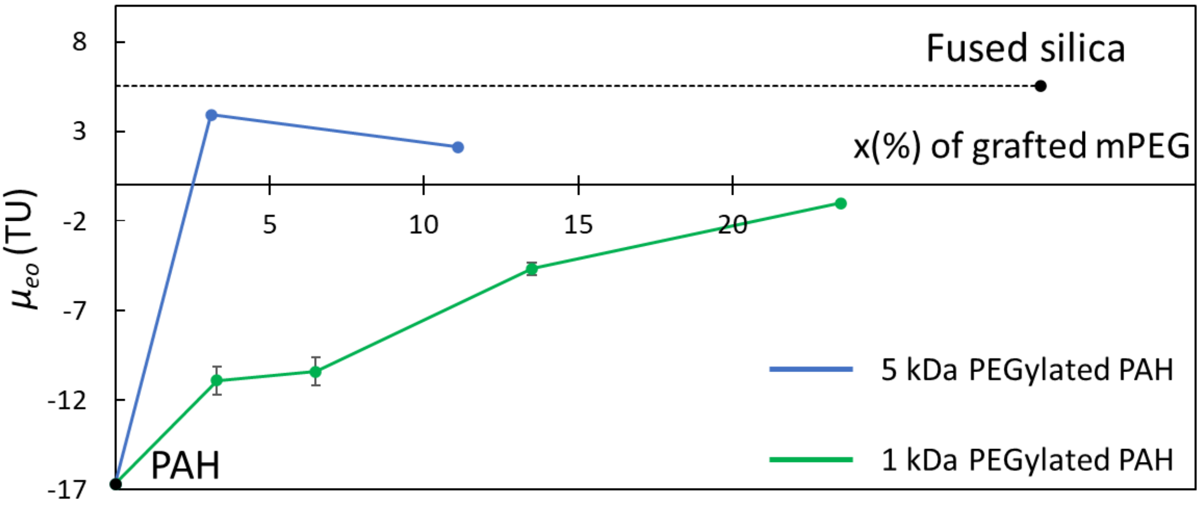
8
3
-2
-7
-12
-17
μ_{eo} (TU)
5
10
15
20
Fused silica
x(%) of grafted mPEG
PAH
5 kDa PEGylated PAH
1 kDa PEGylated PAH

Figure 3

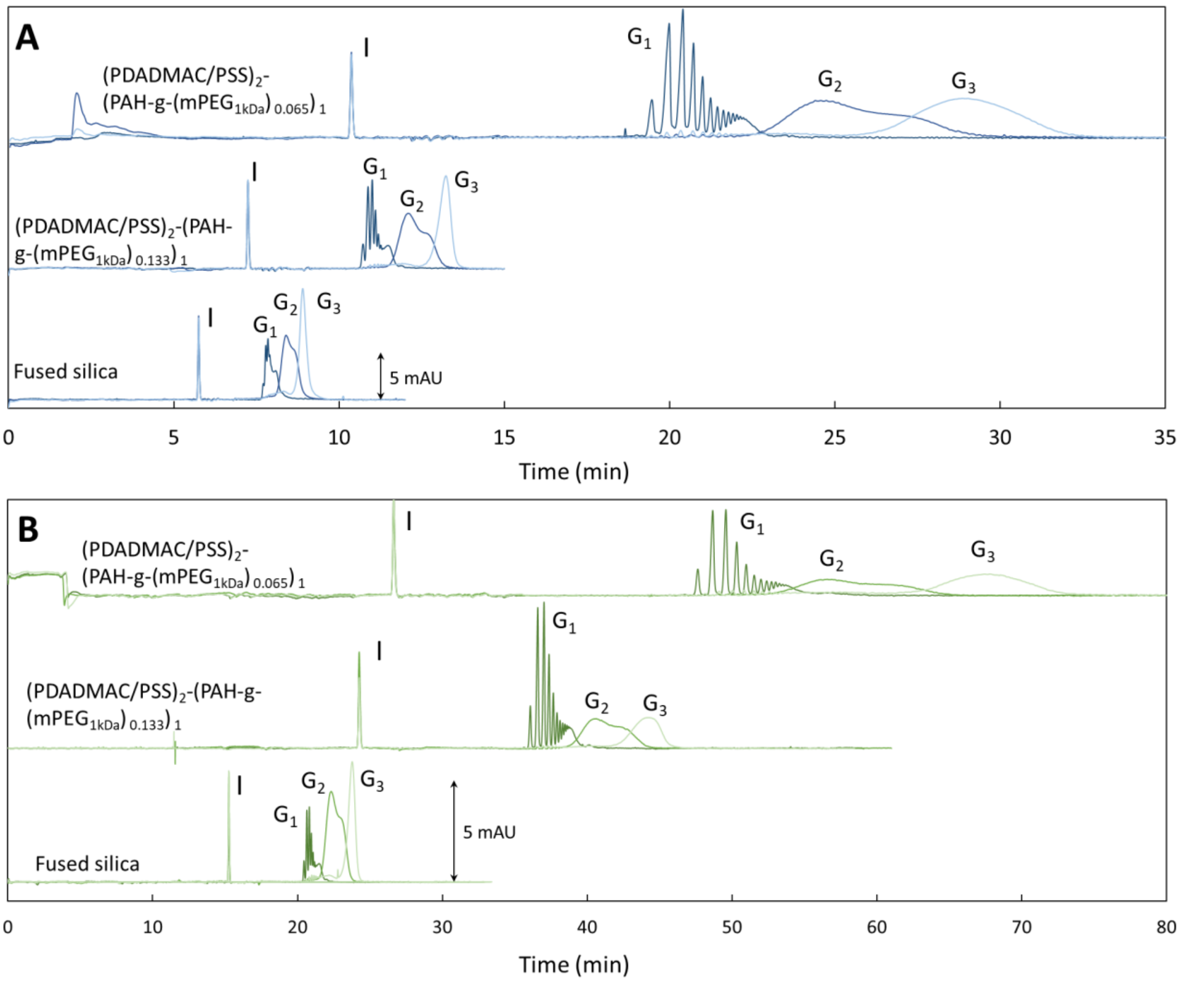
A
(PDADMAC/PSS)$_2$-(PAH-g-(mPEG$_{1kDa}$)$_{0.065}$)$_1$
I
G$_1$
G$_2$
G$_3$
(PDADMAC/PSS)$_2$-(PAH-g-(mPEG$_{1kDa}$)$_{0.133}$)$_1$
I
G$_1$
G$_2$
G$_3$
Fused silica
I
G$_1$
G$_2$
G$_3$
5 mAU
0
5
10
15
20
25
30
35
Time (min)
B
(PDADMAC/PSS)$_2$-(PAH-g-(mPEG$_{1kDa}$)$_{0.065}$)$_1$
I
G$_1$
G$_2$
G$_3$
(PDADMAC/PSS)$_2$-(PAH-g-(mPEG$_{1kDa}$)$_{0.133}$)$_1$
I
G$_1$
G$_2$
G$_3$
Fused silica
I
G$_1$
G$_2$
G$_3$
5 mAU
0
10
20
30
40
50
60
70
80
Time (min)

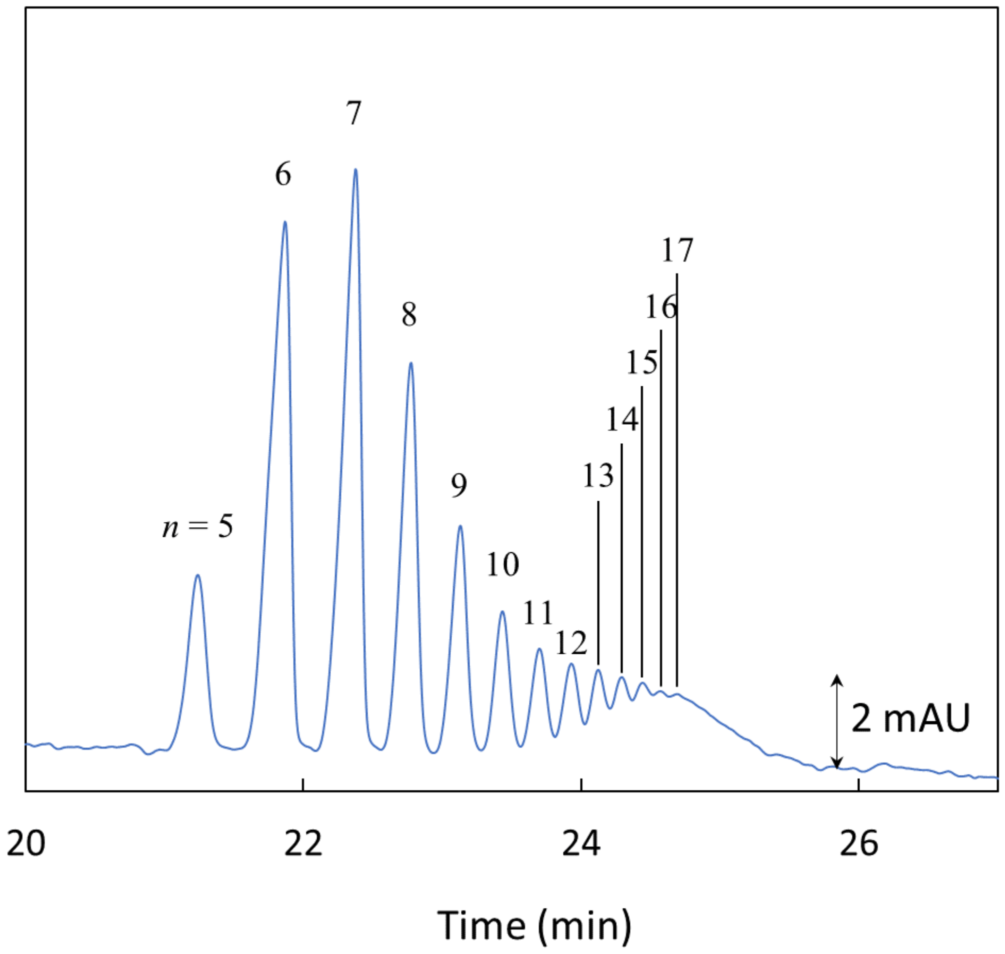
n = 5
6
7
8
9
10
11
12
13
14
15
16
17
2 mAU
20
22
24
26
Time (min)

Figure 5

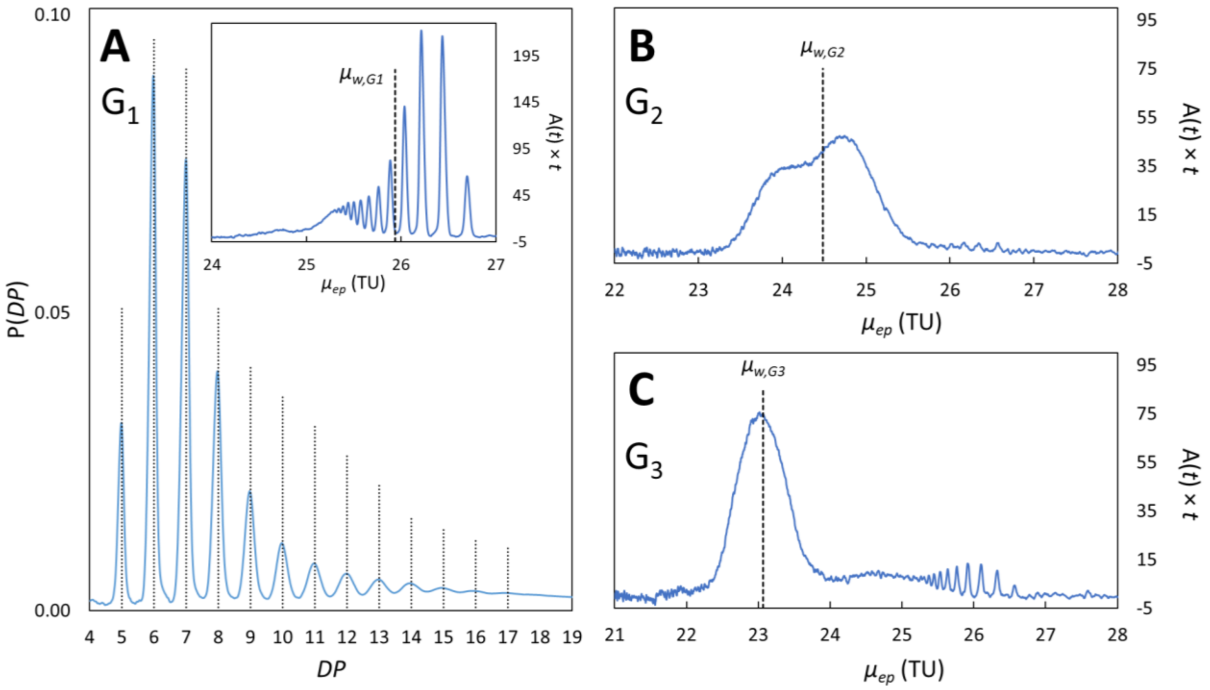
A
G$_1$
P(DP)
0.10
0.05
0.00
4 5 6 7 8 9 10 11 12 13 14 15 16 17 18 19
DP
$\mu_{w,G1}$
195
145
95
45
-5
A(t) × t
24 25 26 27
μ_{ep} (TU)
B
G$_2$
$\mu_{w,G2}$
95
75
55
35
15
-5
A(t) × t
22 23 24 25 26 27 28
μ_{ep} (TU)
C
G$_3$
$\mu_{w,G3}$
95
75
55
35
15
-5
A(t) × t
21 22 23 24 25 26 27 28
μ_{ep} (TU)

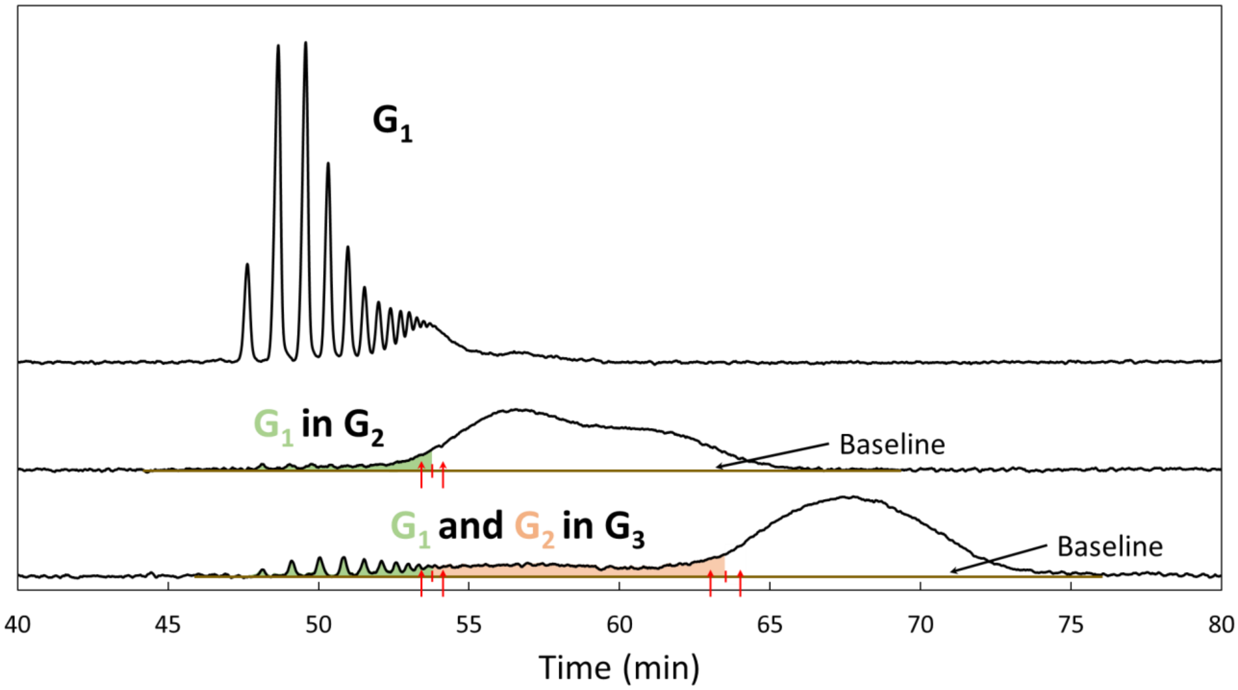
G_1
G_1 in G_2
Baseline
G_1 and G_2 in G_3
Baseline
40
45
50
55
60
65
70
75
80
Time (min)

Table 1: Molar mass, hydrodynamic radius, and effective charge of the three first generations of DGL.

	G_1	G_2	G_3
M_w (gmol^{-1}) [43]	1 720	11 800	32 100
DP_n [41]	8	48	123
R_h (nm) [41]	1.03	1.96	3.06
Effective charge (z_{eff}) [50]	7	31	43

Table 2: Targeted and effective grafting ratio of the PEGylated poly(allylamine).

Polycation backbone	mPEG 1kDa				mPEG 5kDa	
	3%	6%	12%	20%	5%	20%
PAH	3.3[a]	6.5[a]	13.3[a]	23.5[a]	3.1[b]	11.1[b]

[a] Grafting rates determined by ^1H NMR

[b] Grafting rates determined by SEC-MALLS

Table 3: PDI_M and PDI_μ values for DGL G_1, G_2 and G_3. Error bars are ± one SD ($n = 3$).

G_1					G_2			G_3		
DP_w	PDI_M	μ_w	σ_μ	PDI_μ (10^{-4})	μ_W	σ_μ	PDI_μ (10^{-4})	μ_W	σ_μ	PDI_μ (10^{-4})
7.66 ± 0.04	1.09 ± 0.05	26.05 ± 0.09	0.49 ± 0.02	3.61 ± 0.3	24.39 ± 0.1	0.50 ± 0.02	4.28 ± 0.36	23.28 ± 0.18	0.33 ± 0.01	1.97 ± 0.18